35th AIAA Fluid Dynamics Conference and Exhibit, 6 - 9 June 2005, Toronto, Canada AIAA2005-4757

Numerical Simulation of Flow Around the Colorado Micro Aerial Vehicle

D. Gyllhem*, K. Mohseni†, D. Lawrence‡,
Research and Engineering Center for Unmanned Vehicles,
Department of Aerospace Engineering,
University of Colorado, Boulder, CO 80309-429.

P. Geuzaine§
CENAERO, Avenue Jean Mermoz 30, 6041 Gosselies, Belgium.

Micro aerial vehicles (MAVs) are distinguished by their small size, low aspect ratio, and low velocity. As a result, MAVs fly at low Reynolds number flow regimes with significant drag characteristics and strong tip vortices. This investigation is focused on the aerodynamic characteristics of a recently developed MAV at the University of Colorado. The Colorado MAV has a flexible membrane wing with an aspect ratio of 1.2 and a chord of 0.27 m. Numerical simulations of the flow around the Colorado fixed wing MAV are presented using a steady state parallel compressible Navier-Stokes solver. The computational grid has 510,000 nodes and about 3 million tetrahedral elements. The maximum calculated lift coefficient is approximately 1.2. The airplane stall angle is at 30°. The high stall angle is attributed to the enhanced lift from a low pressure region above the wing caused by strong tip vortices. Minimum drag coefficient was calculated to be 0.06 at 2° angle of attack. A laminar separation bubble is formed on the upper surface of the wing at moderate angle of attack. The drag increases rapidly as the angle of attack increases. A maximum aerodynamic efficiency of $L/D = 4$ is observed when flying at 10 m/s.

I. Introduction

Micro Aerial Vehicles (MAVs) are small flying aircraft with various applications from surveillance to sensor networking. MAVs have attracted significant attention since mid-1990's for both civilian and military applications. In 1992, when the smallest airplanes in use were the Uninhibited Aerial Vehicles (UAVs) with a wingspan on the order of one meter, Hundley and Gritton suggested that it would take only 10 years for one to develop a 1 cm wingspan vehicle that can carry a 1 gram payload.[1] It is clear that this goal has not been achieved, mostly because of lack of knowledge of MAV aerodynamics. MAVs operate in flow regimes with Reynolds numbers below 200,000. Another aerodynamic signature of MAVs is wings with small aspect ratio; in most cases the chord is roughly equal to the wingspan. This combination of low Reynolds number flight and low aspect ratio wings results in a flow regime totally alien to conventional aircraft. Although

*Graduate student, currently at the Royal Institute of Technology, Stockholm, SE, 100-44, Sweden.
†Assistant Professor, AIAA member. Corresponding author mohseni@colorado.edu
‡Associate Professor, AIAA Member
§Group Leader, AIAA member.

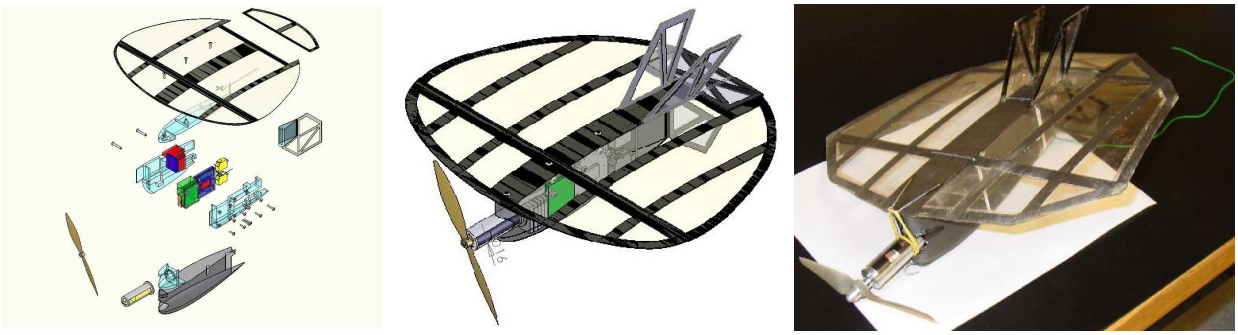

(a) (b) (c)

Figure 1. Colorado MAV, a flexible wing micro air vehicle designed, fabricated, and tested at the University of Colorado. (a) CAD model assembly, (b) CAD model, (c) CMAV prototype.

small birds and insects fly under these conditions, this is a relatively new flight environment for man-made aircraft.

In order for required MAV capabilities to be realized, several areas will need more focused attention. The absence of sophisticated computational analysis methods, lack of commercially available micro-electro-mechanical actuators, and the difficulties associated with accurate experimental work at this scale have all restricted research. From a system and manufacturing standpoint, technological advances in microfabrication techniques and in the miniaturization of electronics in the last decade promise to make MAVs feasible.

One of the most interesting and least understood aspects of MAV flight is the aerodynamics.[2,3,4,5,6] Unsteady aerodynamics play a significant role in MAV flight and stability. Furthermore, the small mass of MAVs make them susceptible to atmospheric turbulence and gusty wind conditions. In order to generate enough lift, flight stability, and performance, MAV designs require novel aerodynamic concepts. This manuscript reports on recent progress in numerical aerodynamic simulation of a fixed-wing MAV at the University of Colorado (CMAV).[7]

II. Colorado MAV Design

Recently a flexible wing MAV was designed and built (see Figure 1) at the University of Colorado. CMAV is designed to serve as a platform for characterizing the flight performance of different low Reynolds number wing designs by measuring the in-flight accelerations due to control inputs and gusts. The platform houses an on-board flight computer and communications system that can process sensor information, transmit data to a ground station, and control the aircraft via pilot input from the ground station. Three-axis accelerations can be measured using an on-board Inertia Measurement Unit (IMU). In addition, CMAV has proven to be an excellent educational tool. A great deal of insight into the subtleties of MAV design has been gained through the process of engineering a working MAV, and the current platform serves as a useful base for continuing development.

The airframe of CMAV consists of a low aspect ratio elliptical membrane wing with an integrated elevator at the trailing edge, two angled vertical stabilizers attached ahead of the elevator, a fuselage below the wing that houses the electronics and propulsion system, and a rudder attached to the trailing edge of the fuselage. The wing is a cambered-plate design with a root chord of 27 cm and a span of 30 cm and a wing area of 7.74×10^{-2} m^2. The camber profile is taken from a reduced-thickness Eppler 387 airfoil, and the wing is unswept, has no dihedral and no geometric twist. CMAV is launched by hand and lands without landing gear.

CMAV specifications are summarized in the Table 1. Maximum lift coefficient is 1.2 based on the value from 2D airfoil data. This gives a stall speed of 6 m/s. The angle of attack at stall is 17 deg from XFOIL based on the aspect ratio and the airfoil coordinate data.

The wing is constructed from narrow strips of prepreg carbon fiber that form structural ribs. This design was inspired by the successful design used on the MAVs constructed by the University of Florida.[8] The wing structure is covered by a single layer of Saran film, which has proven to be very light-weight, strong and easy to repair. The fuselage is also made from prepreg carbon fiber, and machined high-density foam pieces inside the fuselage hold the electronics and motor in place.

Span	30 cm
Root Chord	27 cm
Airfoil	Eppler 387
Aspect ratio	1.2
Wing planform	Zimmerman
Camber	3.78%
Sweep,Dihedral	0°
Pitch control	Elevator integrated into wing
Yaw control	Rudder behind fuselage
Airfoil stall angle	17° (XFOIL)
Max. Speed	13 m/s
Max Load factor	4.96 g
Weight	0.170 kg

Table 1. The data of the original Colorado MAV configuration.

III. Computational Approach

Waszak *et al.*[9] and Viieru *et al.*[10] demonstrated that the aerodynamic performance of membrane wing is comparable to that of a rigid wing. Since the computational cost of a rigid wing is significantly lower than that of a flexible wing, we will focus on the rigid wing simulations in this study. The solver used in this study is a domain decomposition based parallel three-dimensional compressible Euler and Navier-Stokes solver which combines finite volume and finite element discretizations on unstructured tetrahedral meshes. It features an upwind scheme using a piecewise linear reconstruction of the flow variables in each control volume for the convective term, and a P1 finite element Galerkin approximation for the diffusive term.[11,12] Both convective and diffusive terms are evaluated with edge-based formula. The solver uses the AOMD (Algorithm Oriented Mesh Database) library[13] for the management of the topological mesh entities across multiple processors. Pseudo time-integration is performed for steady state flows with the backward Euler scheme. Since this scheme is implicit, the flow solver must solve at each time-step a system of nonlinear equations. For this purpose, it relies on an inexact Newton method using a finite difference GMRES solver preconditioned by a restricted additive Schwarz algorithm.[14,15]

For simplicity, the propeller is not simulated in the current investigation. Starting from the CAD model shown in Figure 1(b) the viscous grid is built in three steps. First a triangular surface mesh is constructed around the CAD model of the MAV. Stretched tetrahedral elements are then constructed outside of the fuselage to capture the boundary layer close to the surface. The refinement on the leading and trailing edges of the wing as well as on the engine can be observed in these figures. Finally, regular tetrahedral elements are constructed toward the outside sphere boundary; see Figure 2(c). Inviscid grids are generated by skipping the second stage. The final viscous mesh has 510,000 points with 3 million tetrahedral elements.

CFD Validation. The accuracy of the compressible solver was verified by comparison of the results of the flow over a flat plate at an angle of attack with experimental data from Muller.[16] A flat plate with a chord of 8 inches and a span of 12 inches is investigated. The AR is 1.5 and the plate has a rounded leading edge and a tapered trailing edge. Simulations are carried at Reynolds number of 140,000. The CAD model of the plate, shown in Figure 3, is then used to generate an unstructured mesh with 320,000 nodes and 1.9 million tetrahedral elements. The mesh is intentionally refined in the vicinity of the leading and trailing edges. The results from the steady state compressible solver are shown in Figure 4. The numerical results are

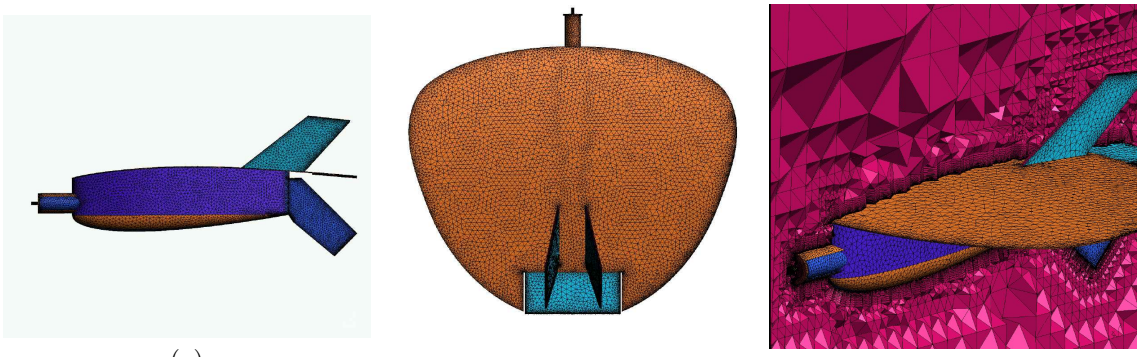

(a) (b) (c)

Figure 2. Computational grid around the CMAV. (a) Sideview (b) Topview (c) a cut through the centerline of the volume.

slightly conservative as compared with the experimental data. Higher stall angle and $C_{L,max}$ are predicted by the CFD model. This might be due to inherent disturbances in the experimental setup that could trigger unsteady flow and earlier stall. The drag polar is predicted nicely but with a shift in the drag at zero lift.

IV. CMAV Simulation Results

Steady state CFD simulations around the Colorado MAV are reported in this section. Lian *et al.*[17] reports less than 1% difference between the steady and unsteady computations around a similar MAV even at high angles of attack. Converged solutions are reported when the relative computational residual drops to less than 10^{-4}. The current simulations are stiff. To alleviate this, solutions were initially constructed with a constant variation of the variables within each control volume. Then the flow field using the linear reconstruction is started from the converged constant solution rather than a uniform flow field.

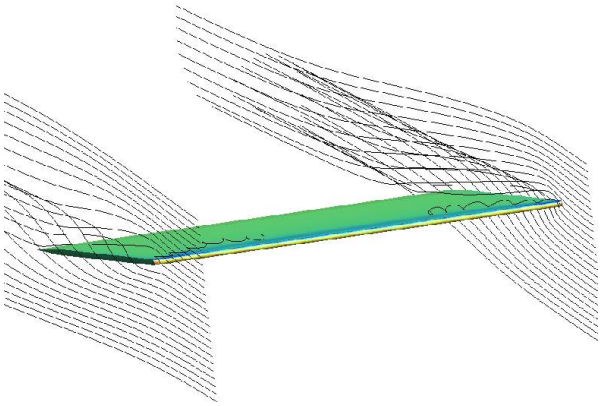

Figure 3. Streamlines around the edges of a flat plate. A streamline is caught up in the separation vortex above the plate.

Lift and Drag. As shown in Figure 5, the lift results show a linear increase with the AoA until the stall angle. Due to a the small cambered wings in the Colorado MAV, the lift coefficient at 0° incidence is around $C_L = 0.05$. The MAV velocity is relatively low and is varied in the range of 6 m/s $< u_\infty <$ 14 m/s. As a result the lift coefficient does not change significantly for the considered air speeds. Because of the small aspect ratio of 1.2, the Colorado MAV can have a relatively high AoA before stall at 30°. This is attributed to strong tip vortices that create a low pressure region on the upper surface of the wing. Since the tip vortices have a comparable size with the wing, they have a significant effect on the lift enhancement in MAVs.[10] The stall characteristics of the current MAV are not as abrupt as those on fast flying larger delta wings. One can expect further delay in stall when flexible wings are used. Ifju[18] reports a delayed stall angle of 20° in wind tunnel tests of a flexible wing MAV

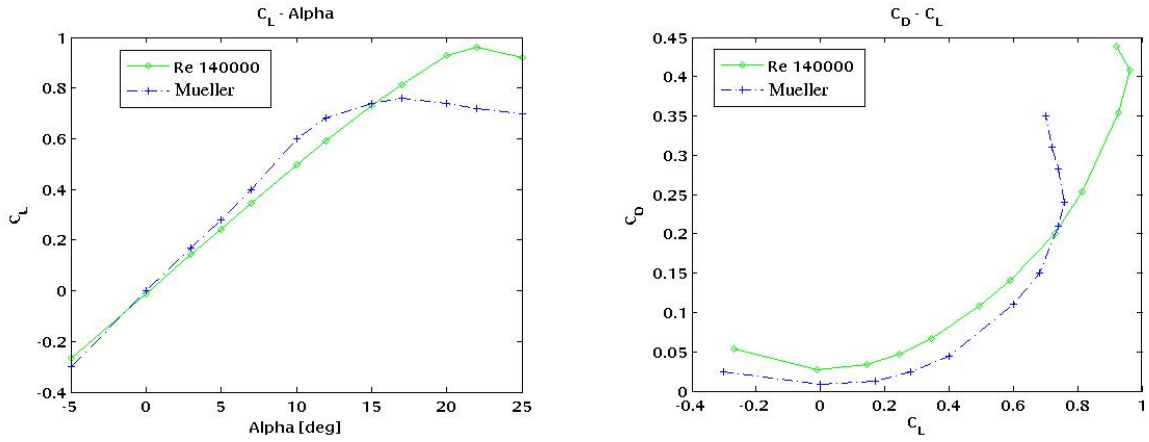

(a) (b)

Figure 4. Validation of the compressible code on a flat plate (a) lift curve (b) drag polar.

with AR of 2. Previously reported results in Lian *et al.*[17] show a stall angle of 49° on a rigid wing MAV with AR around 1. Consequently one can conclude that the stall angle increases by decreasing the AR and by adopting a wing with flexibility.

The drag of the Colorado MAV is affected by the fuselage and the vortices created at the wing tips as shown in Figure 5. To fly with minimum drag the plane should have an AoA of 2° which corresponds to $C_L = 0.15$. This gives a total minimum drag coefficient $0.04 < C_{Dmin} < 0.08$ for the full 3D configuration, depending on the airspeed.

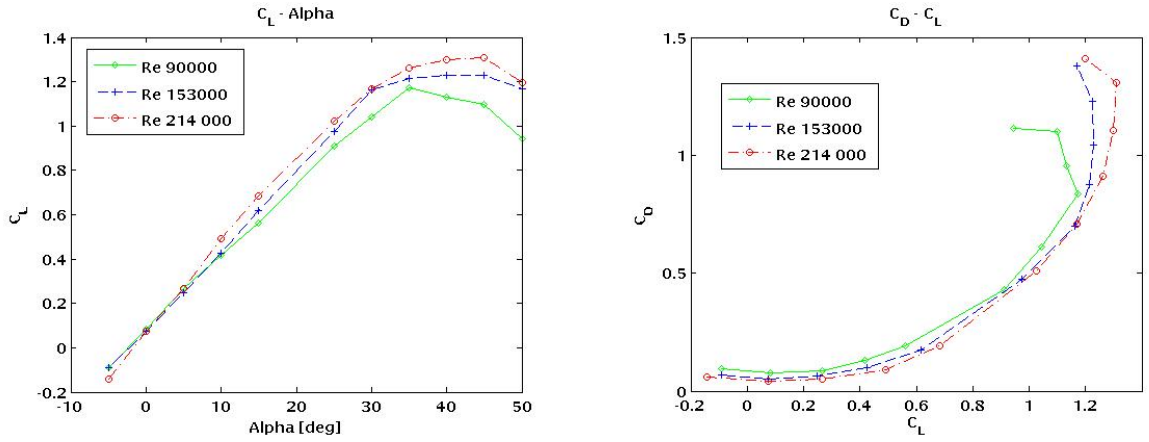

(a) (b)

Figure 5. (a) Lift coefficient - alpha (b) Drag coefficient - Lift coefficient

Separation Bubbles. Laminar separation bubbles, occurring at low Reynolds numbers, strongly influence the performance of almost all MAVs by significantly reducing L/D. The separation bubble is caused by the laminar boundary layer separation on the top surface of the wing where a strong adverse pressure gradient exists. Velocity drop toward the trailing edge of the wing results in a pressure rise on the wing's top surface. Laminar separated flows are sensitive to disturbances which could lead to transition to a turbulent flow. If the pressure gradient is not very strong the flow can reattach as a turbulent boundary layer. The volume

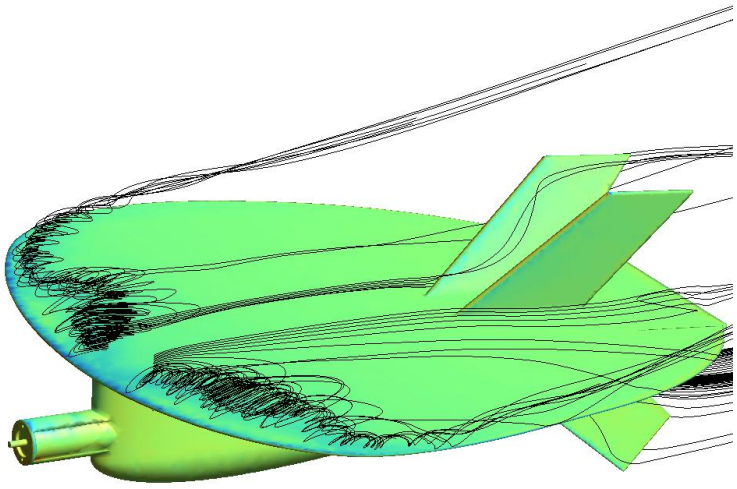

Figure 6. The streamlines getting caught up in the reversed vortex on the upper surface.

enclosed by the region of separated laminar flow and turbulent flow is called a laminar separation bubble. Inside the bubble the flow may be circulating. There is almost no energy exchange with the outer flow, which makes the laminar separation bubble quite stable.

The effective thickness of the boundary layer in a separated flow is much larger than unseparated ones, which results in increased drag. Laminar separation bubbles can also change the lift and moment characteristics of a wing, which can lead to instability and control problems. Forced or natural transition can be used to avoid drag penalties and nonlinear behavior of lift and moment coefficients. Turbulators can be employed just before the region of laminar separation to cause forced transition to a turbulent flow. Turbulent flows have higher momentum and can follow the surface curvature better than the associated laminar flows. Furthermore, by appropriately shaping the airfoil geometry one can enforce transition to occur in front of the main pressure recovery region, where the bubble might occur.

Figure 6 shows the extent of the separation bubble in our simulation for an incidence of 15°. This is also evident in the chordwise pressure profile in Figure 7 in the form of a pressure irregularity at the leading edge.

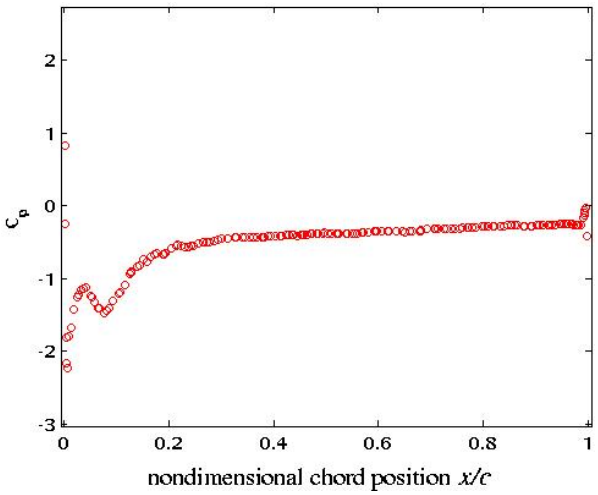

Figure 7. Chordwise pressure distribution. The separation bubble present at the pressure graph as a pressure disturbance.

Tip Vortices. The pressure difference between the upper and lower surfaces of a wing that is operating at a positive lift can create tip vortices. As shown in Figure 8 the flow particles from the lower wing surface (higher pressure) will move toward the upper surface at a lower pressure. The vortex is strong at the tips and decreases rapidly to zero at midspan. The tip vortices will eventually diffuse in the ambient. Tip vortices play a significant role in low aspect ratio MAVs and their effects are manifested in various ways. The vortices

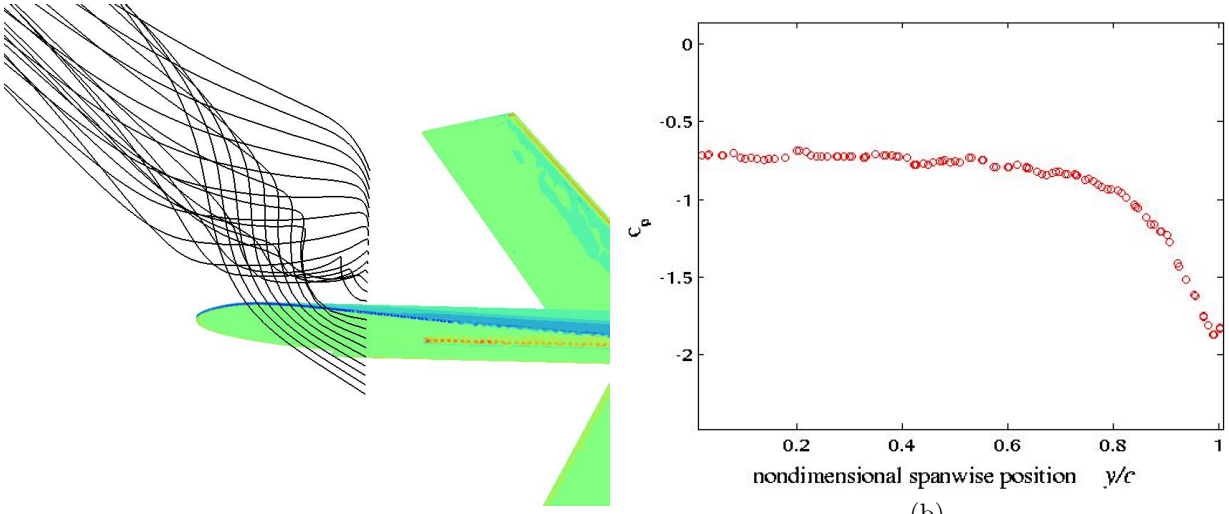

(a) (b)

Figure 8. Tip vortex structure at an incidence of 30 degrees, (a) visualization (b) pressure coefficient in spanwise direction.

induce downwash movement that decrease the effective AoA over the wing, resulting in a component of the total force on the wing in the drag direction (induced drag), and which leads to lower lift. On the other hand, the extra low pressure on the upper surface results in delayed stall and an increase in lift. Tip vortices can also increase the drag due to the generated lift and can cause roll instability. Investigations on tip vortices in MAVs have been reported by Viieru *et al.*[10]

Tip vortices increase in strength as the AoA is increased. Pressure distribution on the upper surface of the wing is reported in Figure 8(b) at a position of $x/c = 0.26$ and AoA of 30°. As seen in the figure, the tip vortices have a significant influence on the pressure coefficient on more than 40% of the wing span, resulting in more lift generation. On the other hand, larger tips vortices results in larger induced drag. To this end, Viieru *et al.*[10] showed that the lift to drag ratio is lower at the tip region of a low AR wing.

Aerodynamic Efficiency. Figure 9 shows the aerodynamic efficiency. The maximum L/D is achieved at 7° AoA and it is calculated to be 3.2 for flight at a speed of 5.88 m/s. If the airspeed is increased to the maximum speed of around 14 m/s the L/D can reach a value of 5.5. Flying the MAV at an angle of attack under 4° or above 15° results in a poor efficiency. It appears that the efficiency is less sensitive to the airspeed as the angle of attack increases. This is mainly due to the fact that while the lift increases, the drag increases quadratically so the L/D decreases faster for a higher airspeed. A wind tunnel analysis of the Florida MAV[17] gives a maximum L/D of 3 at 7.5° AoA at $Re = 70,000$. Improving the aerodynamic efficiency is an important step to enhance endurance of MAVs.

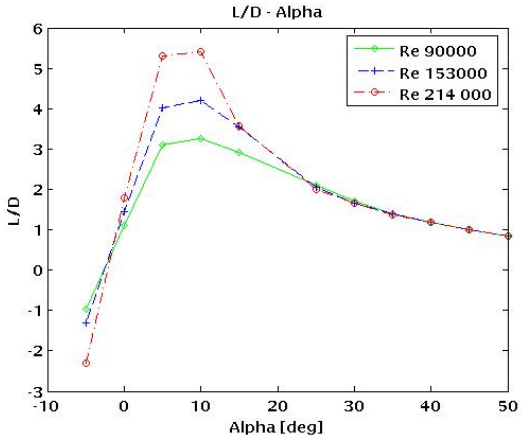

Figure 9. Aerodynamic efficiency for the three Reynolds numbers investigated.

Turbulence Modeling. The compressible solver uses the one-equation turbulence model of Spalart-Allmaras.[19] Figures 10 and 11 show the results for simulations with and without this model. Results for simulations around the wing-only with no fuselage or rudder are also reported in these figures. All the computations are at a Reynolds number of 153,000 which corresponds to a flight speed of 10 m/s. Application of the turbulence model appears to slightly increase the lift prediction. However, significant variations are found in stall prediction where the simulations with the turbulence model predicts $C_{Lmax} = 1.4$ while without a turbulence model $C_{Lmax} = 1.2$ is reported at the same stall angle of 30°. This might be due to numerical dissipation associated with the numerical technique used in the computational solver.

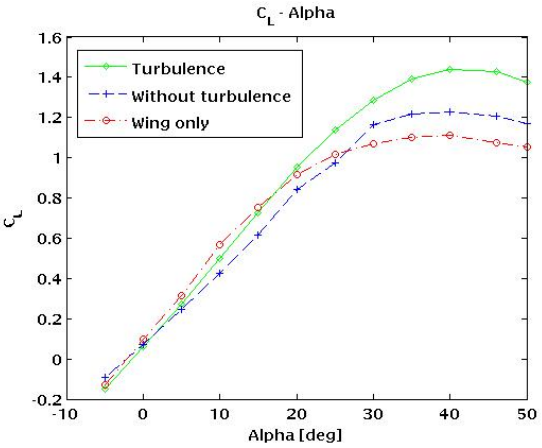

Figure 10. Comparison of lift curves between turbulence model, without turbulence model and the geometry with a wing only.

When simulating the flow around the wing-only configuration (with no stabilizers or fuselage) the lift curve is seen to have the same initial slope. However, stall occurs at an AoA of 20°. This also results in a lower $C_{Lmax} = 1.1$. These results show that the body and the stabilizers of the MAV helps in the creation of lift, which is remarkable. Essentially the fuselage acts as a guide for the flow which results in improved stall characteristics.

As seen in Figure 11 the wing-only has a lower minimum drag than the full MAV. The C_{D0} of the wing is in fact only 22% of the whole aircraft geometry. Lower drag of the wing is less pronounced at higher angles of attack. Viieru *et al.*[10] used endplates to help probe the tip vortex effects. They confirmed that for small AoA the endplate can reduce the downwash movement due to the tip vortices and therefore increase the effective angle of attack and the lift. At larger AoA the tip vortices are so strong that the endplate cannot significantly affect the lift.

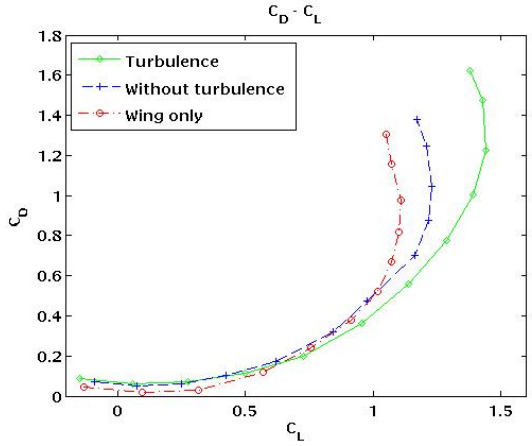

Figure 11. Drag polar comparison.

V. Conclusion

Numerical simulations of the flow around a recently developed micro aerial vehicle at the University of Colorado (CMAV) are reported. Aerodynamic characteristics of the CMAV are presented. It is found that the maximum aerodynamic efficiency is achieved at about 7° AoA for Reynolds numbers between 90,000 and 214,000. Laminar separation bubbles are observed on the top surface of the wing at these Reynolds numbers. Effects of tip vortices on the aerodynamic performance is also investigated. The airplane stall angle is at 30°. The high stall angle of CMAV is attributed to strong tip vortices. Minimum drag coefficient was calculated to be 0.06 at 2° angle of attack. A maximum aerodynamic efficiency of $L/D = 4$ is observed when flying at 10 m/s. The maximum aerodynamic efficiency is observed to increase with increasing flying speed.

Acknowledgments

The research in this paper was partially supported by the NSF contract 427947 and the AFOSR contracts F49620-02-1-0176 and FA9550-05-1-0334.

References

[1]W.R. Davis, B.B. Kosicki, D.M., and D.F. Kostishack. Micro air vehicles for optical surveillance. *MIT Lincoln Lab Journal*, 9(2):197–214, 1996.

[2]Y.S. Lian, S.Y. Wei, P.G. Ifju, and E. Verron. Membrane wing model for micro air vehicles. *AIAA J.*, 41(12):2492–2494, 2004.

[3]T.J. Mueller, editor. *Fixed and Flapping Wing Aerodynamics for Micro Air Vehicle Applications*, Reston, Virginia, 2001. American Institute of Aeronautics and Astronautics.

[4]W. Shyy, M. Berg, and D. Ljungqvist. Flapping and flexible wings for biological and micro air vehicles. *Progress in Aerospace Sciences*, 35:455–505, 1999.

[5]T.J. Mueller and J.D. Delaurier. Aerodynamics of small vehicles. *Ann. Rev. Fluid Mech.*, 35:89–111, 2003.

[6]R.J. Templin. The spectrum of animal flight: Insects to pterosaurs. *Progress in Aerospace Sciences*, 36:393–436, 2000.

[7]K. Mohseni, D. Lawrence, D. Gyllhem, M. Culbreth, and P. Geuzaine. Flow simulation around a micro air vehicle in a plume characterization scenario. AIAA paper 2004-6598, American Institute of Aeronautics and Astronautics, *3rd* Unmanned Unlimited Technical Conference, Workshop and Exhibit, September 20-22 2004.

[8]P.G. Ifju, D.A. Jenkins, S. Ettinger, Y. Lian, W. Shyy, and M.R. Waszak. Flexible-wing-based micro air vehicles. AIAA paper 2002-0705, January 2002. 40^{th} Aerospace Sciences Meeting & Exhibit, Reno, Nevada.

[9]M.R. Waszak and L.N. Jenkins. Stability and control properties of an aeroelastic fixed wing micro aerial vehicle. AIAA paper 2001-4005, August 2001. AIAA Atmospheric Flight Mechanics Conference, Montreal, Canada.

[10]D. Viieru, Y. Lian, W. Shyy, and P.G. Ifju. Investigation of tip vortex on aerodynamic performance of a micro air vehicle. AIAA paper 2003-3597, 2003.

[11]A. Dervieux. Steady Euler simulations using unstructured meshes. In *Proceedings of the VKI Lectures Series 1985-04, 16th Computational Fluid Dynamics*, von Karman Institute, Brussels, Belgium, March 1985.

[12]T. J. Barth. Numerical aspects of computing high Reynolds number flows on unstructured meshes. AIAA paper 91-0721, January 1991.

[13]J.F. Remacle and M. S. Shephard. An algorithm oriented mesh database. *International Journal for Numerical Methods in Engineering*, 58:349–374, 2003.

[14]P. Geuzaine. Newton-Krylov strategy for compressible turbulent flows on unstructured meshes. *AIAA Journal*, 39(3):528–531, 2001.

[15]X. C. Cai, C. Farhat, and M. Sarkis. A minimum overlap restricted additive Schwarz preconditioner and applications in 3D flow simulations. *Contemporary Mathematics*, 218:478–484, 1998.

[16]T.J. Mueller. Aerodynamic measurements at low reynolds numbers for fixed wing micro-air vehicles. In *Development and Operation of UAVs for Military and Civil Applications*. VKI, Belgium, September 13-17, 1999.

[17]Y. Lian, W. Shyy, D. Wiieru, and B. Zhang. Membrane wing aerodynamics for micro air vehicles. *Prog. in Aero. Sci.*, 39(6-7):425–465, 2003.

[18]R.M. Wasak, D.A. Jenkins, and P.G. Ifju. Stability and control properties of an aeroelastic fixed wing micro aerial vehicle. AIAA paper 2002-4005, 2001.

[19]P.R. Spalart and S.R. Allmaras. A one-equation turbulence model for aerodynamic flows. *La Recherche Aerospatiale*, 1:5–21, 1994.